Nano Research
DOI 10.1007/s12274-016-1273-9
Research Article
ISSN 1998-0124
CN 11-5974/O4

Highly efficient and multidimensional extraction of targets from complex matrices using aptamer-driven recognition

Jie Wang[1], Haijing Shen[1], Chi Huang[1], Qinqin Ma[1], Yaning Tan[1], Fenglei Jiang[1], Chao Ma[2], and Quan Yuan[1] (✉)

[1] *Key Laboratory of Analytical Chemistry for Biology and Medicine (Ministry of Education), College of Chemistry and Molecular Sciences, Wuhan University, Wuhan 430072, China*
[2] *Hefei National Laboratory for Physical Sciences at the Microscale, University of Science and Technology of China, Hefei 230026, China*

Received: 26 June 2016
Revised: 5 August 2016
Accepted: 31 August 2016

KEYWORDS

aptamer,
adsorbent,
selectivity,
separation,
extraction

ABSTRACT

Adsorbents are widely employed in both fundamental and applied research areas such as separation technology, biotechnology, and environmental science. Selectivity and reusability are two most important requirements for adsorbents. Aptamers exhibit perfect selectivity and easy regeneration, which make them uniquely effective adsorption materials. Herein, we have rationally designed novel aptamer-based adsorbents and investigated their performance in extraction/separation of targets from an aqueous solution. These adsorbents can selectively extract targets from complicated sample matrices containing background compounds. Moreover, they can also be easily recycled without a significant loss of adsorption capacity. Notably, the adsorbents did not affect the activity of isolated biological samples, revealing their potential for the purification/separation of biomolecules. Composite adsorbents were constructed using aptamer-based adsorbents and a porous polymer, displaying highly efficient target separation from aqueous solution. Finally, separation columns were constructed, and targets in the aqueous solution were efficiently separated by these columns. The aptamer-based adsorbents described here exhibit great promise for potential applications in separation technology, biotechnology, and environment-related areas.

1 Introduction

Adsorption is one of the most commonly encountered phenomena in our daily life that has attracted broad interest during the past decades [1–6]. Undoubtedly, it is a very useful technique, with first practical applications dated to ancient times. Nowadays, the rapidly developing adsorption techniques are widely employed in separation technology [7], biotechnology [8], environmental science [9–16], and catalysis [17]. Separation technology, e.g., solid-phase extraction, usually employs adsorbents to extract targets from

Address correspondence to yuanquan@whu.edu.cn

complicated sample matrices or pre-concentrate them from dilute solutions to improve detection sensitivity [18]. Biotechnology uses adsorbents to purify biomolecules such as proteins, nucleic acids, and even intact cells directly from crude samples [8]. Besides, adsorption is one of the most convenient methods of environmental science for removing pollutants from wastewater [10]. Obviously, adsorption is of great importance for both fundamental and applied research. Although adsorbents are utilized in different application areas, they share some key requirements, i.e., good selectivity and reusability [2, 18].

Over the past several years, single-stranded DNA and RNA (aptamers) have emerged as a novel class of molecules that attract extensive attention, since they are capable of recognizing a broad range of substances with high affinity and specificity, ranging from metal ions and small molecules to tissues [19–25]. Compared to other functional biomolecules such as antibodies and enzymes, aptamers offer the advantages of design flexibility, synthetic accessibility, easy modification, and chemical stability [26–30]. Several particularly important features of aptamers make them uniquely efficient components of adsorption materials, namely perfect selectivity and easy regeneration. According to previous studies, aptamers specifically bind their targets with pico- to nanomolar dissociation constants by folding into unique secondary or tertiary structures that accommodate the molecular structure of the targets [31–37], revealing their ability to extract even low concentrations of targets in the presence of background compounds from sample matrices. Furthermore, the unique structures of aptamers can be efficiently denaturized by changing pH or increasing the temperature to release the captured targets into desired media and the functional aptamers can be easily regenerated within minutes [38, 39], indicating their good reusability as adsorbents.

Herein, we have rationally designed a novel class of adsorbents with good selectivity and reusability by employing aptamers as binding groups. Specifically, these adsorbents were constructed by immobilizing aptamers on the surface of superparamagnetic magnetic nanoparticles (MNPs). These adsorbents feature good selectivity due to the special binding pockets of aptamers and good reusability due to the rational integration of their easy regenerability with magnetic separation. It is worth noting that adsorbents for inorganic metal ions, organic molecules, and even intact living cells can be easily obtained by simply changing the types of aptamers used. In addition, unmodified MNPs can also be used as adsorbents to separate phosphate from aqueous solution. Composite adsorbents and separation columns were further constructed to investigate the potential applications (e.g., affinity chromatography) of these adsorbents in device fabrication. The strategy described here may therefore not only serve as a promising method for the design of novel adsorbents, but also expand the application of aptamers in separation technology, biotechnology, and environmental science.

2 Experimental

2.1 Synthesis of mesoporous TiO_2 ($mTiO_2$)-coated Fe_3O_4 nanoparticles (Fe_3O_4@$mTiO_2$ MNPs)

To synthesis the nanoparticles, $FeCl_3 \cdot 6H_2O$, trisodium citrate, and sodium acetate were first dissolved in ethylene glycol. The solution was then transferred into a Teflon-lined stainless steel autoclave and heated at 200 ℃ for 10 h. Subsequently, the as-prepared Fe_3O_4 nanoparticles, concentrated ammonia solution, and tetrabutyl titanate were added to ethanol, and the mixture was ultrasonicated for 15 min. The solution was allowed to react at 45 ℃ for 24 h under continuous mechanical stirring. The resulting products were dried and calcined at 500 ℃ for 2 h to obtain Fe_3O_4@$mTiO_2$ MNPs.

2.2 Fabrication of aptamer-based adsorbents

MNPs were immersed in an acetone solution of 3-aminopropyltriethoxysilane (APTES) (5%) for 10 h to introduce amino groups onto their surface. Subsequently, a bifunctional cross-linker (Sulfo-SMCC) was used to functionalize MNPs with aptamers. MNPs (10 mg) and cross-linker (succinimidyl 4-(N-maleimidomethyl)cyclohexane-1-carboxylate, Sulfo-SMCC) (4 mg) were reacted in 2-(N-morpholino)-ethansulfonic acid (MES) buffer (20 mM, pH 6.8) for 4 h. The resulting product was collected and washed. The obtained MNPs and aptamer (20 nmol) were

added to a phosphate buffer saline (20 mM, pH 7.2), and the solution was shaken at room temperature for 24 h. The as-prepared aptamer-functionalized MNPs were magnetically separated and washed with distilled water for subsequent use.

2.3 Selectivity tests

Briefly, Apt-Hg-MNPs (1 mg) were dispersed in Tris-nitrate buffer (1 mL, 10 mM, pH 8.0) containing Hg^{2+} (1 ppm), Na^{+} (10 ppm), Ca^{2+} (10 ppm), Cu^{2+} (10 ppm), Cd^{2+} (10 ppm), Zn^{2+} (10 ppm), and Ag^{+} (10 ppm). The above solution was allowed to react for 2 h at room temperature. The adsorbents were isolated, and the resulting solution was collected to determine the residual concentrations of each ion. Additionally, Apt-BPA-MNPs (1 mg) were suspended in Tris-nitrate buffer containing bisphenol A (BPA, 60 ppm), bisphenol F (BPF, 60 ppm), benzoic acid (60 ppm), phenol (60 ppm), and hydroxybenzoic acid (60 ppm). The solution was treated with Apt-BPA-MNPs obtained above. Further, Apt-SA-MNPs (1 mg) were mixed with ~10^5 CFU/mL *Staphylococcus aureus (S. aureus)* in 1 mL of stroke-physiological saline solution and incubated for 2 h. The supernatant was collected to determine the residual number of *S. aureus* by plate count. An *Escherichia coli (E. coli)* sample (~10^5 CFU/mL) was also treated with Apt-SA-MNPs using the same procedure.

2.4 Cyclic separation of Hg^{2+}, BPA, and *S. aureus*

Taking the cyclic separation of Hg^{2+} as an example, Apt-Hg-MNPs (1 mg) were dispersed in a solution of Hg^{2+} (1 mL, 1 ppm, pH 8.0, Tris-nitrate buffer), and the mixture was allowed to react for 2 h at room temperature. Subsequently, Apt-Hg-MNPs were separated, and the amount of residual Hg^{2+} was determined. The separated Apt-Hg-MNPs were washed with HCl (pH 3) and deionized water for three times to remove the adsorbed Hg^{2+} ions, and the regenerated Apt-Hg-MNPs were used to separate Hg^{2+} ions from another aqueous solution. Cyclic removal of BPA (60 ppm) and *S. aureus* (~10^5 CFU/mL) was carried out using the same procedure.

2.5 Cyclic separation of PO_4^{3-}

Typically, MNPs (1 mg) were added to a solution of sodium dihydrogen phosphate (1 mL, 1 ppm), and the mixture was allowed to react at room temperature for 2 h. The MNPs were separated and washed with acetonitrile (50%) and trifluoroacetic acid (0.1%) before being used in the next cycle. The concentration of PO_4^{3-} was measured using the ammonium molybdate spectrophotometric method according to the National Standard of the People's Republic of China (GB 11893-89).

2.6 Preparation of composite adsorbents

Briefly, Apt-Hg-MNPs (1 mg) were dispersed in acetic acid solution (5 mL, 0.1 M), followed by the addition of chitosan powder (100 mg). Subsequently, a solution of β-glycerol 2-phosphate disodium salt hydrate (β-GP) (500 μL, 0.26 M) was added upon cooling in an ice-water bath. Finally, the mixture was heated to 37 ℃ in an oven to produce the composite adsorbents. The related adsorbents for BPA and PO_4^{3-} were fabricated using the same protocol.

2.7 Separation of Hg^{2+}, BPA, and PO_4^{3-} using composite adsorbents

In a typical experiment, the composite adsorbent for mercury was added to a Tris-nitrate buffer containing Hg^{2+} ions (1 ppm). The solution was incubated at room temperature for 2 h under continuous mechanical stirring. Subsequently, the composite adsorbent was separated, and the solution was used for the following color reactions. Separation of BPA and PO_4^{3-} was achieved using the same method. Dithizone, ferric trichloride, and ammonium molybdate were utilized to form colored complexes with Hg^{2+}, BPA, and PO_4^{3-}, respectively.

2.8 Fabrication of separation columns

Separation columns were fabricated using plastic medical syringes (10 mL) as containers for the composite adsorbents. The acidic suspension was prepared employing the abovementioned methods, followed by addition of the β-GP solution. The composite hydrogel was formed by transferring the above solution into plastic syringes, and the resultant filters were heated to 37 ℃ in an oven. Separation columns for Hg^{2+}, PO_4^{3-}, BPA, and *S. aureus* were fabricated separately, using the corresponding adsorbents.

2.9 Removal of Hg^{2+}, BPA, and PO_4^{3-} by the separation columns

Briefly, the aqueous solution containing Hg^{2+} (1 mL, 1 ppm) was allowed to pass through the syringe filters under the action of gravity, and the filtrate was collected to determine the residual Hg^{2+} concentration. The separation of BPA (60 ppm), PO_4^{3-} (1 ppm), and *S. aureus* (~10^5 CFU/mL) was performed using the same procedure.

3 Results and discussion

The approach used to construct aptamer-based adsorbents is illustrated in Fig. 1(a). Core–shell MNPs were prepared by coating Fe_3O_4 nanoparticles with a layer of mesoporous titanium dioxide [40]. The TiO_2 shell can adsorb phosphate due to the classic coordination reaction between titanium ions and PO_4^{3-}, with the amount of available active binding sites greatly increased by the mesoporous structure of TiO_2. More importantly, the abundant hydroxy groups on the surface of TiO_2 can be used to introduce amino groups via hydrolysis of 3-aminopropyltriethoxysilane [41]. Thiol groups at the 3′-end of aptamers and the amino groups on the MNP surface were further linked by a bifunctional cross-linker (Sulfo-SMCC) to obtain the final adsorbents [42]. In this study, three kinds of aptamers binding Hg^{2+} (designated as Apt-Hg) [43], bisphenol A (designated as Apt-BPA) [44], and

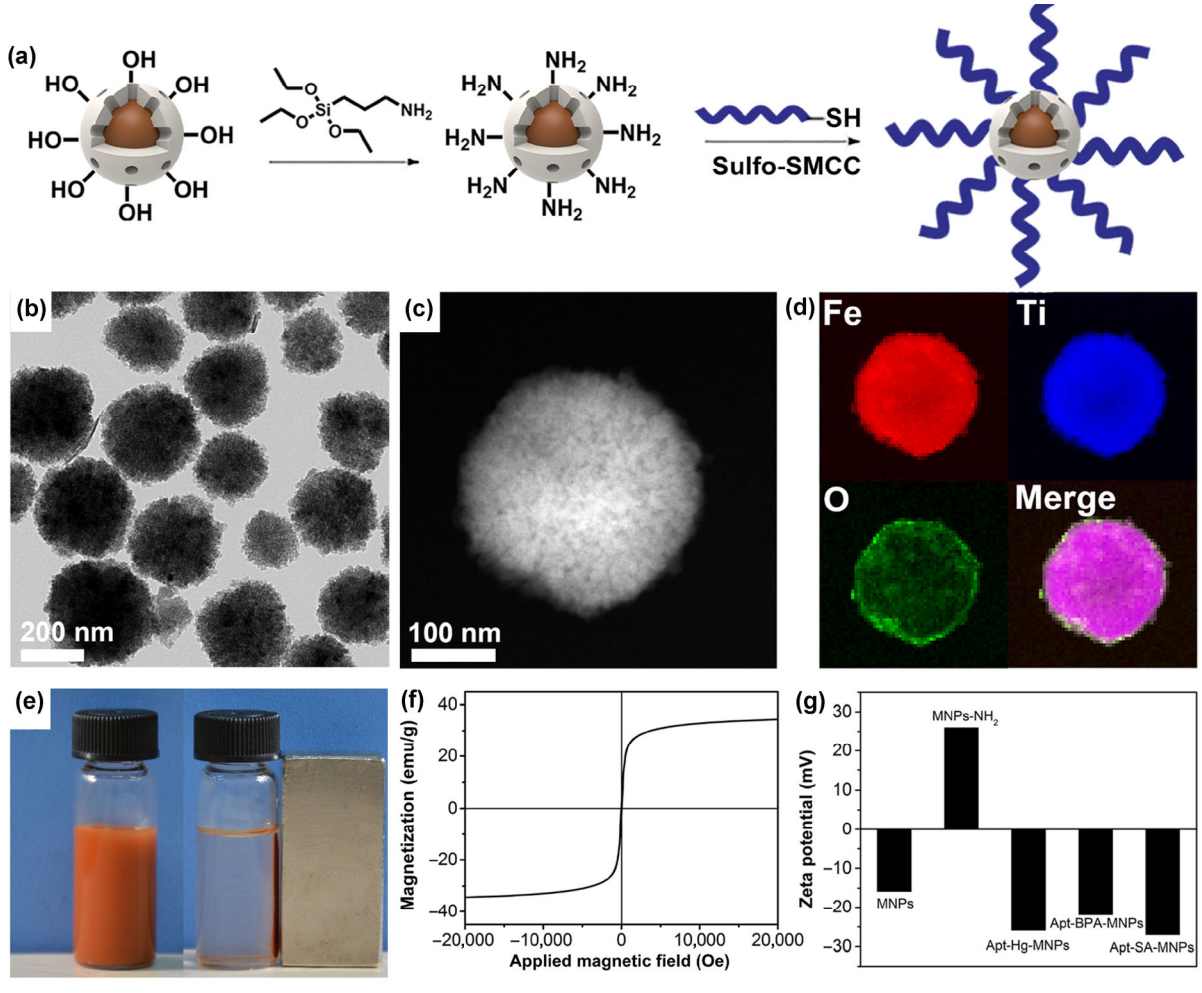

Figure 1 Characterization of adsorbents. (a) Schematic preparation of aptamer-based adsorbents. TEM (b), HAADF-STEM (c), and elemental mapping (d) images of adsorbents. (e) Aqueous dispersion of adsorbents and the separation test using a permanent magnet. (f) Magnetization field dependence plot of the adsorbents. (g) Zeta potentials of MNPs, amino-functionalized MNPs, Apt-Hg-MNPs, Apt-BPA-MNPs, and Apt-SA-MNPs.

S. aureus (designated as Apt-SA) [45] were immobilized on the surface of MNPs to construct the corresponding adsorbents (designated as Apt-Hg-MNPs, Apt-BPA-MNPs, and Apt-SA-MNPs). The sequences of these aptamers were as follows:

Apt-Hg: 5′-CTT CTT TCT TCC CCT TGT TTG TTG CCC CCC CCC-SH-3′

Apt-BPA: 5′-CCG GTG GGT GGT CAG GTG GGA TAG CGT TCC GCG TAT GGC CCA GCG CAT CAC GGG TTC GCA CCA TTT TTT TTT-SH-3′

Apt-SA: 5′-TCC CTA CGG CGC TAA CCC CCC CAG TCC GTC CTC CCA GCC TCA CAC CGC CAC CGT GCT ACA AC TTT TTT TTT-SH-3′

Transmission electron microscopy (TEM), high-angle annular dark-field scanning transmission electron microscopy (HAADF-STEM), and magnetization and zeta potential measurements were performed to characterize aptamer-based adsorbents. TEM imaging showed that the adsorbents having an average particle diameter of ca. 250 nm were well dispersed (Fig. 1(b)). HAADF-STEM images (Fig. 1(c)), elemental mapping (Fig. 1(d)), and line scan analysis (Fig. S6 in the Electronic Supplementary Material (ESM)) show that a thick layer of TiO_2 was grown on the surface of the Fe_3O_4 nanoparticles. The image in Fig. 1(e) suggests that aptamer-based adsorbents can be well dispersed in solution and be completely collected within minutes (<2 min) using a permanent magnet, implying the possibility of efficient extraction/separation. Magnetization measurements were performed to characterize the magnetic properties of adsorbents and evaluate their magnetic separation effectiveness. As shown in Fig. 1(f), the magnetization saturation value was determined to be 34.4 emu/g, and the magnetic hysteresis loops clearly showed that MNPs exhibited no remanence, revealing the superparamagnetic character of these adsorbents. This superparamagnetism can allow the combination of different adsorbents with good dispersibility in aqueous solution due to the absence of magnetic interactions between them. Besides, these superparamagnetic adsorbents can also rapidly respond to external magnetic fields, since they can quickly generate a higher magnetic flux density compared to ferromagnetic materials. Zeta potential measurements were performed to verify the successful immobilization of aptamers on the surface of MNPs. As shown in Fig. 1(g), the MNPs were negatively charged (–15.9 mV) due to the presence of surface hydroxyl groups, developing a high positive charge (26.0 mV) after the introduction of amino groups. Finally, the MNPs became negatively charged after immobilization of aptamers, with the zeta potentials determined to be –25.9 mV for Apt-Hg-MNPs, –21.9 mV for Apt-BPA-MNPs, and –27.0 mV for Apt-SA-MNPs, indicating that aptamers were successfully grafted onto the surface of MNPs.

Unlike traditionally used organic functional groups such as EDTA, aptamers showed little binding affinity towards non-targets, which made them especially appropriate for the extraction of targets from complex matrices. As illustrated in Fig. 2(a), aptamer-based adsorbents were dispersed in sample matrices containing targets and other substances. Once exposed to the targets, the aptamers on the surface of MNPs instantly folded into unique structures to capture the corresponding targets. In contrast, the background compounds in solution were unaffected. The adsorbents could subsequently be collected by an external magnetic field, and the loaded targets could be eluted into the desired medium for further usage. The selectivity of aptamer-based adsorbents was investigated by Hg^{2+} extraction tests, using Apt-Hg-MNPs in the presence of other metal ions. Similarly, Apt-BPA-MNPs were used to extract BPA in the presence of other organic molecules, and Apt-SA-MNPs were utilized to separate *S. aureus* and *E. coli*. As shown in Fig. 2(b), more than 97.53% of Hg^{2+} ions were successfully extracted from the solution, that is, the residual concentration of Hg^{2+} in the sample matrices was 0.026 ppm. In contrast, the concentrations of Na^+, Ca^{2+}, Cu^{2+}, Cd^{2+}, Zn^{2+}, and Ag^+ were virtually unchanged (Fig. S11 in the ESM), suggesting that Apt-Hg-MNPs possessed little binding affinity to non-targets in the sample matrices. As for organic molecules (Fig. 2(c)), Apt-BPA-MNPs could efficiently extract about 99.14% of BPA, exhibiting negligible nonspecific adsorption towards BPF, benzoic acid, phenol, and hydroxybenzoic acid (Fig. S14 in the ESM). Similar results were obtained for large intact cells. As shown in Fig. 2(d), above 99.80% of *S. aureus* were removed from the original solution, while only small amounts of *E. coli* were adsorbed. The above results clearly demonstrate the good selectivity of

aptamer-based adsorbents, attributed to the fact that aptamers bind their targets by forming unique well-accommodating structures. Such selectivity makes these adsorbents especially suitable for the extraction/separation of targets in separation technology and the purification of biological macromolecules from crude samples in biotechnology.

Apart from good selectivity, aptamer-based adsorbents also possessed good reusability. The cyclic separation of targets is illustrated in Scheme 1. The adsorbents were dispersed in an aqueous solution containing the targets of interest, and aptamers on the surface of MNPs formed binding pocket structures once in contact with their targets, leading to specific binding. After capturing the targets, the adsorbents were efficiently isolated using a portable permanent magnet. The collected adsorbents were then regenerated by denaturation of the aptamers, resulting in the release of captured targets into the desired media at high concentrations. The regenerated adsorbents could be further used in the next separation cycle.

Cyclic tests were performed to separate Hg^{2+} and BPA and test the feasibility of this design using the corresponding adsorbents. As shown in Fig. 3(a), Hg^{2+} was efficiently separated in all of the ten cycles with removal efficiencies above 90%, clearly suggesting that Apt-Hg-MNPs can be easily recycled without a significant loss of adsorption capacity. Such good reusability was ascribed to the easy regeneration of aptamers and the superior magnetic separation effectiveness of MNPs. Similar results were also obtained for BPA, which could be removed with efficiencies higher than 98.7% (Fig. 3(b)) in all of the tested cycles. The above results thus revealed that aptamer-based adsorbents for metal ions and organic molecules showed good reusability, being promising for practical applications in separation technology or environmental science.

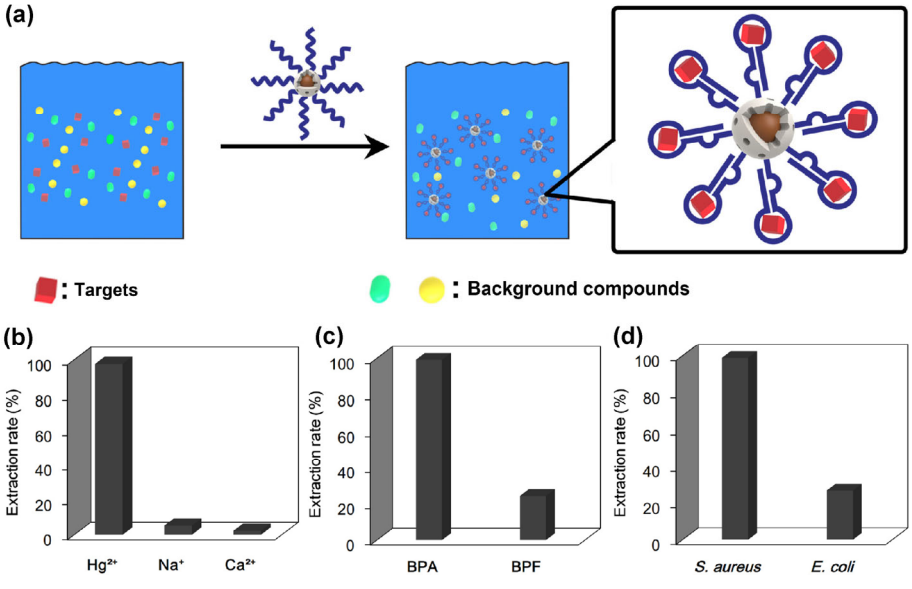

Figure 2 Selectivity tests. (a) Schematic representation of selective target extraction. Extraction efficiencies of aptamer-based adsorbents towards targets and background compounds in selectivity tests for Hg^{2+} (b), BPA (c), and *S. aureus* (d).

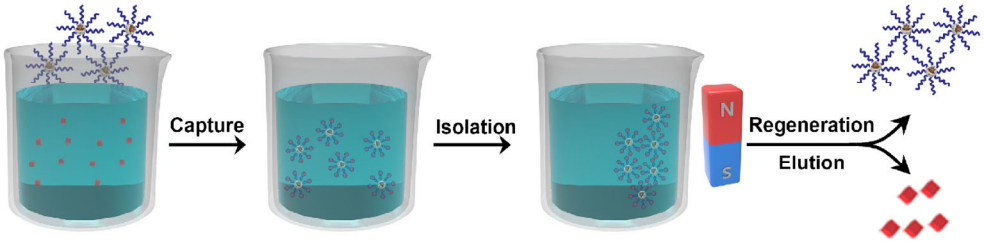

Scheme 1 Schematic representation of the cyclic separation of targets from aqueous solution.

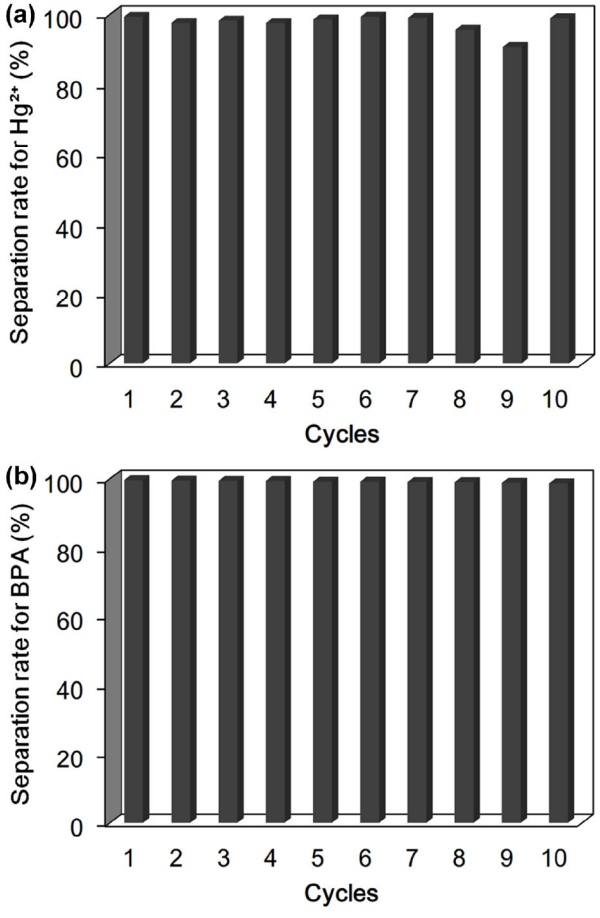

Figure 3 Cyclic extraction of Hg^{2+} and BPA. Cyclic separation efficiencies of aptamer-based adsorbents towards Hg^{2+} (a) and BPA (b) in ten cycles.

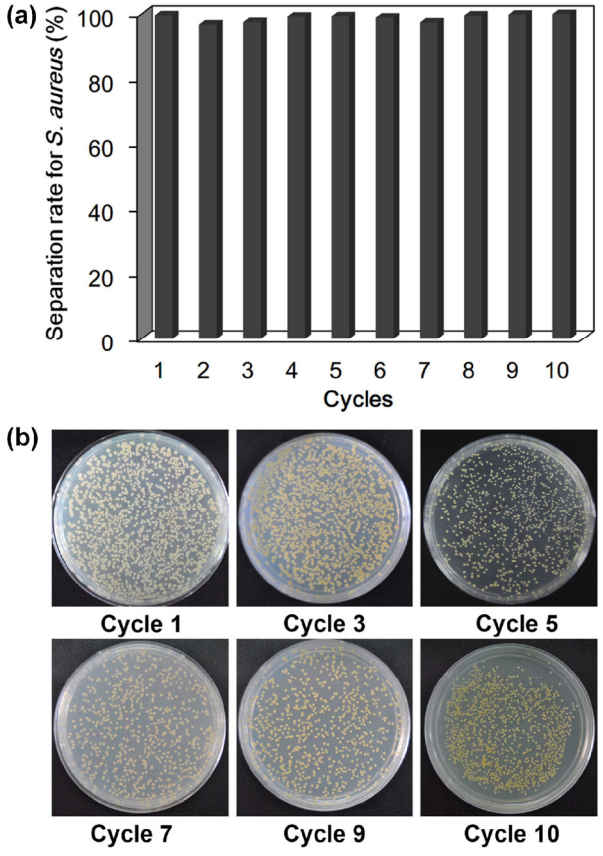

Figure 4 Cyclic separation of *S. aureus*. (a) Cyclic separation efficiencies of aptamer-based adsorbents towards *S. aureus* in ten cycles. (b) Culturing results of isolated *S. aureus* in cycle 1, 3, 5, 7, 9, and 10.

The results of reusability tests of aptamer-based adsorbents for biological macromolecules are shown in Fig. 4(a). Apt-SA-MNPs exhibited excellent performance in extracting *S. aureus* from aqueous solutions, with efficiencies above 96.8% in all cycles. More importantly, the images of cultured agar plates (cycle 1, 3, 5, 7, 9, and 10) showed extensive growth of the isolated *S. aureus* (Fig. 4(b)), clearly indicating that the adsorbents do not significantly affect the activity of target biological molecules. Such good reusability and activity-friendly properties of these adsorbents highlight their potential for the purification/separation of biomolecules.

The above results clearly show that aptamer-based adsorbents display good selectivity and reusability, suggesting their great potential for practical applications in separation technology, environmental science, and biotechnology.

As mentioned above, the mesoporous TiO_2 layer can adsorb PO_4^{3-} from aqueous solutions. Hence, the cyclic phosphate separation performance of MNPs was also tested. The mechanism for PO_4^{3-} adsorption by mesoporous MNPs is illustrated in Fig. 5(a). The large surface area of the mesoporous structure provides abundant active sites, allowing efficient phosphate binding to MNPs via coordination. The concentration of PO_4^{3-} in aqueous solutions was determined by the ammonium molybdate spectrophotometric method. As shown in Fig. 5(b), the sample absorbance decreased to nearly zero after separation, indicating complete removal of PO_4^{3-} by MNPs. This observation was ascribed to the strong binding affinity of TiO_2 towards PO_4^{3-} and the abundant surface active sites in the mesoporous structures [46]. The results of the cyclic removal of PO_4^{3-} are presented in Fig. 5(c). Similar to the results of the former cyclic tests, PO_4^{3-} was effectively separated from aqueous solutions, with

separation efficiencies exceeding 92% even in the tenth cycle, showing the great potential of the above adsorbents for PO_4^{3-} separation in environmental applications.

Composite adsorbents, consisting of the above aptamer-based adsorbents and three-dimensional (3D) porous polymers, were further constructed. As shown in Fig. 6(a), aptamer-based adsorbents were mixed with a solution of chitosan to form homogeneous dispersions, and this was followed by the addition of β-GP to form porous composite adsorbents [47]. Scanning transmission electron microscopy (STEM) was used to characterize the structure of these composite adsorbents. As shown in Fig. 6(b), the latter exhibited a 3D macroporous structure with interconnected open pores after lyophilization, offering sufficient space

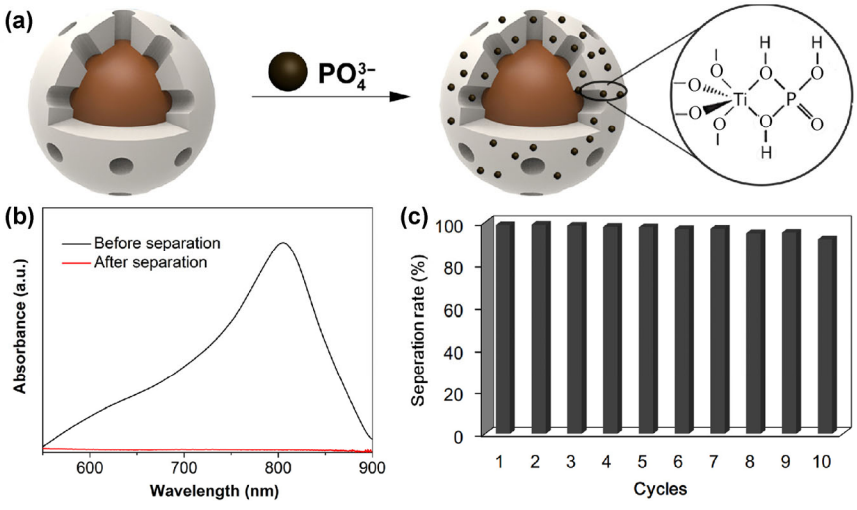

Figure 5 Cyclic separation of PO_4^{3-}. (a) Schematic representation of the adsorption mechanism. (b) UV–Vis absorbance of water samples before (black line) and after (red line) treatment. The absorbance is due to the colored complex formed by PO_4^{3-} and ammonium molybdate. (c) Removal efficiencies of MNPs towards PO_4^{3-} in ten cycles.

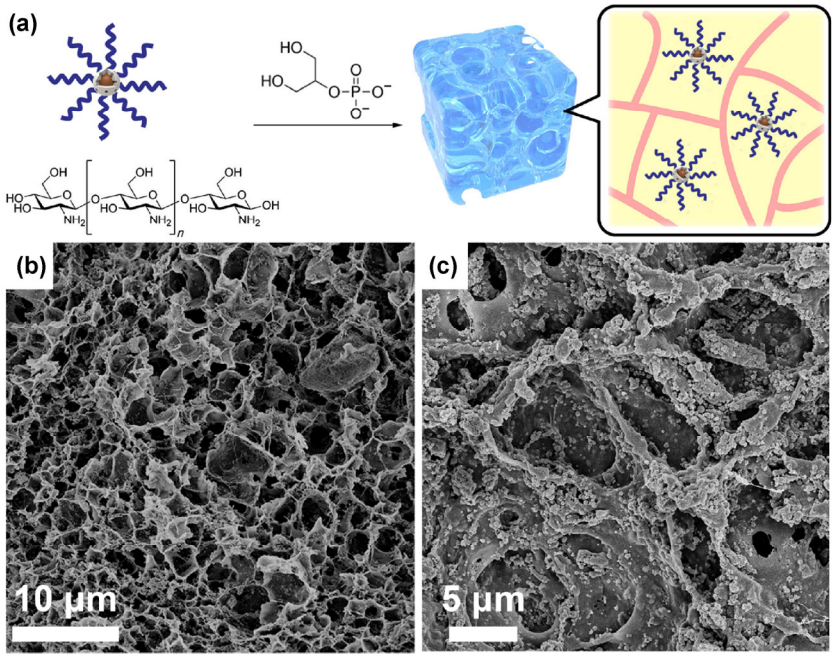

Figure 6 Characterization of composite adsorbents. (a) Schematic fabrication of composite adsorbents. (b) and (c) STEM images of composite adsorbents at different magnifications.

for the diffusion of targets to the binding sites. At higher magnification (Fig. 6(c)), the aptamer-based adsorbents were observed to be well dispersed on the surface of the porous structure, thus, leading to a rough surface morphology of the inner pores. In addition, MNPs were also employed to prepare composite adsorbents for the separation of PO_4^{3-} using the same strategy. Such 3D porous continuous bulk structures were more suited for practical use, e.g., as packing materials in affinity chromatography.

Composite adsorbents containing Apt-Hg-MNPs, Apt-BPA-MNPs, and MNPs were employed to separate Hg^{2+}, BPA, and PO_4^{3-}, respectively, from aqueous solutions. Images of the original and treated solutions are presented in Fig. 7. In order to make the separation results more figurative, dithizone was used to form a colored complex with Hg^{2+}, ferric chloride was utilized to form blue complexes with BPA, and molybdate was utilized to form navy blue complexes with PO_4^{3-}. The organic phase (lower layer) of the original Hg^{2+} solution was dark brown, while the sample treated with the composite adsorbent was light brown, revealing that Hg^{2+} was efficiently separated from the solution. As for BPA, the control solutions were deep blue, while the sample treated with the composite adsorbent was almost colorless, suggesting complete separation. Similar results were also obtained for PO_4^{3-}, where the color of the original and treated solutions showed a remarkable difference due to the high removal efficiency of the composite adsorbent. These results clearly indicated the robust adsorption abilities of the porous composite adsorbents.

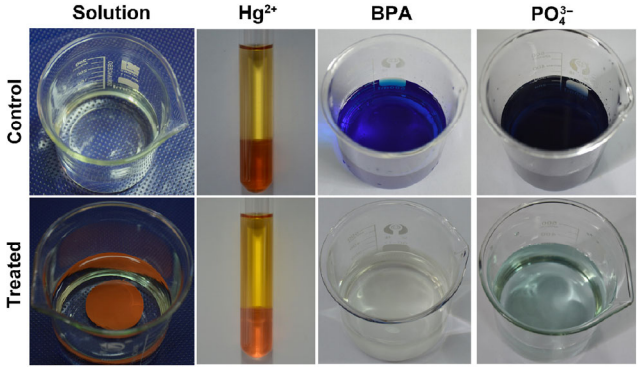

Figure 7 Removal of targets using composite adsorbents. Images of color reactions for Hg^{2+}, BPA, and PO_4^{3-} samples before and after separation. Dithizone, ferric chloride, and molybdate were used to form colored complexes with Hg^{2+}, BPA, and PO_4^{3-}, respectively.

After investigating the separation capabilities of the above composite adsorbents, we constructed separation columns using them as packing materials. The devices were fabricated by transferring the chitosan solution and aptamer-based adsorbents into plastic columns to form composite adsorbents. In such columns, the interconnected pores within these composites allowed the penetration of aqueous solution, while the targets were captured by the adsorbents (Fig. 8(a)). As shown in Fig. 8(b), the residual concentration of Hg^{2+} in the filtrate was 2.46 ppb, indicating that more than 99.75% of Hg^{2+} was separated by the column. Similar results were observed for the separation of BPA, PO_4^{3-}, and *S. aureus*. As shown in Figs. 8(c)–8(e), the residual concentrations of BPA, PO_4^{3-}, and *S. aureus* in the filtrates were ultra-low, and the separation efficiencies of these three targets were above 99.39%, 99.92%, and 99.8%, respectively. The above results clearly displayed the excellent separation performance of the columns, and we anticipated their use for adsorption of targets or interferents in purification/pre-concentration stages of separation technology and environmental science.

4 Conclusions

In summary, this work highlights the fabrication of highly efficient adsorbents based on aptamers. These adsorbents were capable of selectively extracting metal ions, small organic molecules, and even intact cells from complicated sample matrices. More importantly, the adsorbents did not affect the activity of isolated cells. These aptamer-based adsorbents could easily be recycled several times without a significant loss of adsorption capacity. In addition, the separation of phosphate by MNPs was investigated. The MNPs exhibited high separation efficiencies and excellent reusability. Furthermore, aptamer-based adsorbents and MNPs were incorporated into a 3D porous polymer in order to investigate their potential practical applications in device fabrication, and separation columns were constructed. Both the composite hydrogel and the columns displayed excellent separation of targets from aqueous media, revealing the excellent potential of the adsorbents for practical applications. To conclude, the above strategy paves a way for the development of multiple-use aptamer-based adsorbents,

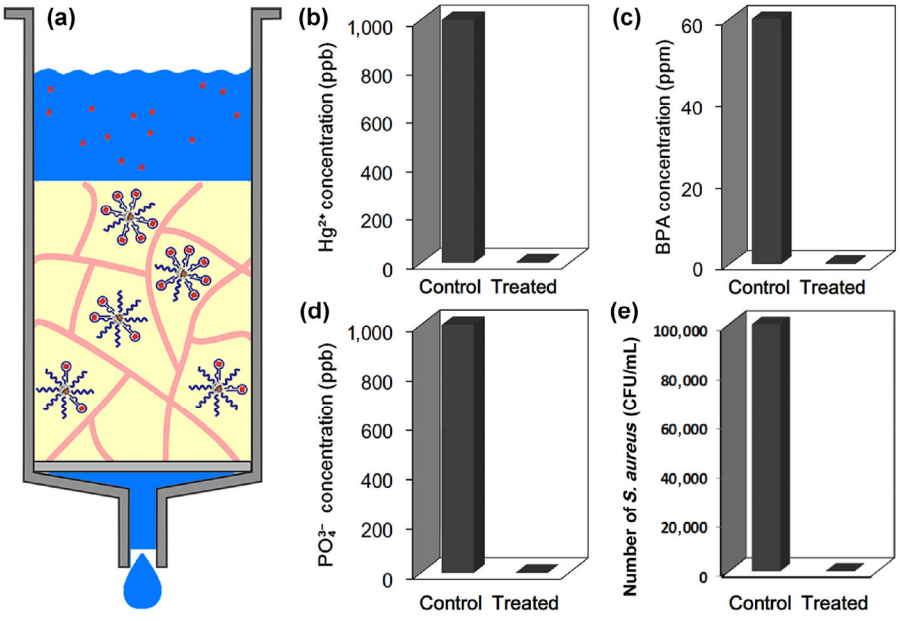

Figure 8 Removal of targets using separation columns. (a) Schematic illustration of the separation columns. Concentrations of Hg^{2+} (b), BPA (c), PO_4^{3-} (d), and *S. aureus* (e) in the samples before and after separation using corresponding columns.

not only promoting the development of materials science, but also providing efficient tools for separation technology, biotechnology, and environmental fields.

Acknowledgements

This work was supported by the National Natural Science Foundation of China (Nos. 51272186 and 21422105), "A Foundation for the Author of National Excellent Doctoral Dissertation of P. R. China" (No. 201220), and Ten Thousand Talents Program for Young Talents. Q. Y. thanks for large-scale instrument and equipment sharing foundation of Wuhan University.

Electronic Supplementary Material: Supplementary material (TEM characterization, line scan analysis, XRD patterns, SEM images) is available in the online version of this article at http://dx.doi.org/10.1007/s12274-016-1273-9.

References

[1] Augusto, F.; Carasek, E.; Silva, R. G. C.; Rivellino, S. R.; Batista, A. D.; Martendal, E. New sorbents for extraction and microextraction techniques. *J. Chromatogr. A* **2010**, *1217*, 2533–2542.

[2] Dąbrowski, A. Adsorption—From theory to practice. *Adv. Colloid Interface Sci.* **2001**, *93*, 135–224.

[3] Deng, Y. H.; Qi, D. W.; Deng, C. H.; Zhang, X. M.; Zhao, D. Y. Superparamagnetic high-magnetization microspheres with an Fe_3O_4@SiO_2 core and perpendicularly aligned mesoporous SiO_2 shell for removal of microcystins. *J. Am. Chem. Soc.* **2008**, *130*, 28–29.

[4] Crane, R. A.; Dickinson, M.; Popescu, I. C.; Scott, T. B. Magnetite and zero-valent iron nanoparticles for the remediation of uranium contaminated environmental water. *Water Res.* **2011**, *45*, 2931–2942.

[5] Lukens, W. W., Jr.; Schmidt-Winkel, P.; Zhao, D. Y.; Feng, J. L.; Stucky, G. D. Evaluating pore sizes in mesoporous materials: A simplified standard adsorption method and a simplified broekhoff-de Boer method. *Langmuir* **1999**, *15*, 5403–5409.

[6] Liu, B. W.; Liu, J. W. DNA adsorption by magnetic iron oxide nanoparticles and its application for arsenate detection. *Chem. Commun.* **2014**, *50*, 8568–8570.

[7] Huang, D. N.; Deng, C. H.; Zhang, X. M. Functionalized magnetic nanomaterials as solid-phase extraction adsorbents for organic pollutants in environmental analysis. *Anal. Methods* **2014**, *6*, 7130–7141.

[8] Borlido, L.; Azevedo, A. M.; Roque, A. C. A.; Aires-Barros, M. R. Magnetic separations in biotechnology. *Biotechnol. Adv.* **2013**, *31*, 1374–1385.

[9] Teng, W.; Wu, Z. X.; Fan, J. W.; Chen, H.; Feng, D.; Lv, Y. Y.; Wang, J. X.; Asiri, A. M.; Zhao, D. Y. Ordered mesoporous

carbons and their corresponding column for highly efficient removal of microcystin-LR. *Energy Environ. Sci.* **2013**, *6*, 2765–2776.

[10] Kalia, S.; Kango, S.; Kumar, A.; Haldorai, Y.; Kumari, B.; Kumar, R. Magnetic polymer nanocomposites for environmental and biomedical applications. *Colloid Polym. Sci.* **2014**, *292*, 2025–2052.

[11] Qu, X. L.; Alvarez, P. J. J.; Li, Q. L. Applications of nanotechnology in water and wastewater treatment. *Water Res.* **2013**, *47*, 3931–3946.

[12] Soto, M. L.; Moure, A.; Domínguez, H.; Parajó, J. C. Recovery, concentration and purification of phenolic compounds by adsorption: A review. *J. Food Eng.* **2011**, *105*, 1–27.

[13] Wu, Z. X.; Li, W.; Webley, P. A.; Zhao, D. Y. General and controllable synthesis of novel mesoporous magnetic iron oxide@carbon encapsulates for efficient arsenic removal. *Adv. Mater.* **2012**, *24*, 485–491.

[14] Wang, J.; Shen, H. J.; Hu, X. X.; Li, Y.; Li, Z. H.; Xu, J. F.; Song, X. F.; Zeng, H. B.; Yuan, Q. A targeted "capture" and "removal" scavenger toward multiple pollutants for water remediation based on molecular recognition. *Adv. Sci.* **2016**, *3*, 1500289.

[15] Wang, P.; Shi, Q. H.; Liang, H. J.; Steuerman, D. W.; Stucky, G. D.; Keller, A. A. Enhanced environmental mobility of carbon nanotubes in the presence of humic acid and their removal from aqueous solution. *Small* **2008**, *4*, 2166–2170.

[16] Huang, P. J. J.; Liu, J. W. Immobilization of DNA on magnetic microparticles for mercury enrichment and detection with flow cytometry. *Chem.—Eur. J.* **2011**, *17*, 5004–5010.

[17] Yokoi, T.; Kubota, Y.; Tatsumi, T. Amino-functionalized mesoporous silica as base catalyst and adsorbent. *Appl. Catal. A: Gen.* **2012**, *421–422*, 14–37.

[18] Xie, L. J.; Jiang, R. F.; Zhu, F.; Liu, H.; Ouyang, G. F. Application of functionalized magnetic nanoparticles in sample preparation. *Anal. Bioanal. Chem.* **2014**, *406*, 377–399.

[19] Bunka, D. H. J.; Stockley, P. G. Aptamers come of age—At last. *Nat. Rev. Microbiol.* **2006**, *4*, 588–596.

[20] Liu, J. W.; Cao, Z. H.; Lu, Y. Functional nucleic acid sensors. *Chem. Rev.* **2009**, *109*, 1948–1998.

[21] Tan, W. H.; Donovan, M. J.; Jiang, J. H. Aptamers from cell-based selection for bioanalytical applications. *Chem. Rev.* **2013**, *113*, 2842–2862.

[22] Pei, H.; Zuo, X.; Zhu, D.; Huang, Q.; Fan, C. Functional DNA nanostructures for theranostic applications. *Acc. Chem. Res.* **2014**, *47*, 550–559.

[23] Fang, X. H.; Tan, W. H. Aptamers generated from Cell-SELEX for molecular medicine: A chemical biology approach. *Acc. Chem. Res.* **2010**, *43*, 48–57.

[24] Hamula, C. L. A.; Guthrie, J. W.; Zhang, H. Q.; Li, X. F.; Le, X. C. Selection and analytical applications of aptamers. *TrAC Trend. Anal. Chem.* **2006**, *25*, 681–691.

[25] Giljohann, D. A.; Mirkin, C. A. Drivers of biodiagnostic development. *Nature* **2009**, *462*, 461–464.

[26] Hamula, C. L. A.; Zhang, H. Q.; Guan, L. L.; Li, X. F.; Le, X. C. Selection of aptamers against live bacterial cells. *Anal. Chem.* **2008**, *80*, 7812–7819.

[27] Liu, Q. L.; Jin, C.; Wang, Y. Y.; Fang, X. H.; Zhang, X. B.; Chen, Z.; Tan, W. H. Aptamer-conjugated nanomaterials for specific cancer cell recognition and targeted cancer therapy. *NPG Asia Mater.* **2014**, *6*, e95.

[28] Song, S. P.; Wang, L. H.; Li, J.; Fan, C. H.; Zhao, J. L. Aptamer-based biosensors. *TrAC Trend. Anal. Chem.* **2008**, *27*, 108–117.

[29] Jayasena, S. D. Aptamers: An emerging class of molecules that rival antibodies in diagnostics. *Clin. Chem.* **1999**, *45*, 1628–1650.

[30] Guo, W.; Hong, F.; Liu, N. N.; Huang, J. Y.; Wang, B. Y.; Duan, R. X.; Lou, X. D.; Xia, F. Target-specific 3D DNA gatekeepers for biomimetic nanopores. *Adv. Mater.* **2015**, *27*, 2090–2095.

[31] Zheng, D.; Seferos, D. S.; Giljohann, D. A.; Patel, P. C.; Mirkin, C. A. Aptamer nano-flares for molecular detection in living cells. *Nano Lett.* **2009**, *9*, 3258–3261.

[32] Mairal, T.; Özalp, V. C.; Sánchez, P. L.; Mir, M.; Katakis, I.; O'Sullivan, C. K. Aptamers: Molecular tools for analytical applications. *Anal. Bioanal. Chem.* **2008**, *390*, 989–1007.

[33] Tombelli, S.; Minunni, M.; Mascini, M. Analytical applications of aptamers. *Biosens. Bioelectron.* **2005**, *20*, 2424–2434.

[34] Liang, H.; Zhang, X. B.; Lv, Y. F.; Gong, L.; Wang, R. W.; Zhu, X. Y.; Yang, R. H.; Tan, W. H. Functional DNA-containing nanomaterials: Cellular applications in biosensing, imaging, and targeted therapy. *Acc. Chem. Res.* **2014**, *47*, 1891–1901.

[35] Tombelli, S.; Minunni, M.; Mascini, M. Aptamers-based assays for diagnostics, environmental and food analysis. *Biomol. Eng.* **2007**, *24*, 191–200.

[36] Palchetti, I.; Mascini, M. Nucleic acid biosensors for environmental pollution monitoring. *Analyst* **2008**, *133*, 846–854.

[37] Huang, P. J.; Liu, J. W. Flow cytometry-assisted detection of adenosine in serum with an immobilized aptamer sensor. *Anal. Chem.* **2010**, *82*, 4020–4026.

[38] Zhao, Q.; Li, X. F.; Le, X. C. Aptamer-modified monolithic capillary chromatography for protein separation and detection. *Anal. Chem.* **2008**, *80*, 3915–3920.

[39] Wang, J.; Wei, Y. R.; Hu, X. X.; Fang, Y. Y.; Li, X. Y.; Liu, J.; Wang, S. F.; Yuan, Q. Protein activity regulation: Inhibition by closed-loop aptamer-based structures and restoration by near-IR stimulation. *J. Am. Chem. Soc.* **2015**, *137*, 10576–10584.

[40] Li, W.; Yang, J. P.; Wu, Z. X.; Wang, J. X.; Li, B.; Feng, S. S.; Deng, Y. H.; Zhang, F.; Zhao, D. Y. A versatile kinetics-controlled coating method to construct uniform porous TiO_2 shells for multifunctional core–shell structures. *J. Am. Chem. Soc.* **2012**, *134*, 11864–11867.

[41] Yuan, Y.; Chen, S.; Paunesku, T.; Gleber, S. C.; Liu, W. C.; Doty, C. B.; Mak, R.; Deng, J. J.; Jin, Q. L.; Lai, B. et al. Epidermal growth factor receptor targeted nuclear delivery and high-resolution whole cell X-ray imaging of Fe_3O_4@TiO_2 nanoparticles in cancer cells. *ACS Nano* **2013**, *7*, 10502–10517.

[42] Yuan, Q.; Wu, Y.; Wang, J.; Lu, D. Q.; Zhao, Z. L.; Liu, T.; Zhang, X. B.; Tan, W. H. Targeted bioimaging and photodynamic therapy nanoplatform using an aptamer-guided G-quadruplex DNA carrier and near-infrared light. *Angew. Chem., Int. Ed.* **2013**, *52*, 13965 –13969.

[43] Dave, N.; Chan, M. Y.; Huang, P. J. J.; Smith, B. D.; Liu, J. W. Regenerable DNA-functionalized hydrogels for ultrasensitive, instrument-free mercury(II) detection and removal in water. *J. Am. Chem. Soc.* **2010**, *132*, 12668–12673.

[44] Jo, M.; Ahn, J. Y.; Lee, J.; Lee, S.; Hong, S. W.; Yoo, J. W.; Kang, J.; Dua, P. Lee, D. K.; Hong, S. et al. Development of single-stranded DNA aptamers for specific bisphenol a detection. *Oligonucleotides* **2011**, *21*, 85–91.

[45] Chang, Y. C.; Yang, C. Y.; Sun, R. L.; Cheng, Y. F.; Kao, W. C.; Yang, P. C. Rapid single cell detection of staphylococcus aureus by aptamer-conjugated gold nanoparticles. *Sci. Rep.* **2013**, *3*, 1863.

[46] Song, H.; Nor, Y. A.; Yu, M. H.; Yang, Y. N.; Zhang, J.; Zhang, H. W.; Xu, C.; Mitter, N.; Yu, C. Z. Silica nanopollens enhance adhesion for long-term bacterial inhibition. *J. Am. Chem. Soc.* **2016**, *138*, 6455−6462.

[47] Zhu, M.; Zhu, Y. F.; Zhang, L. X.; Shi, J. L. Preparation of chitosan/mesoporous silica nanoparticle composite hydrogels for sustained co-delivery of biomacromolecules and small chemical drugs. *Sci. Technol. Adv. Mat.* **2013**, *14*, 045005.